Role of Flow Visualization in the Development of UNICORN

Roquemore, W. M.*[1] and Katta, V. R.*[2]

*[1] Air Force Research Laboratory, Wright-Patterson Air Force Base, OH 45433-7103, USA.
*[2] Innovative Scientific Solutions, Inc., 2766 Indian Ripple Road, Dayton, OH 45440-3638, USA.

Abstract : This paper describes how visualizations have been used in the development and evaluation of a reacting-flow-simulation model known as UNICORN (UNsteady Ignition and COmbustion with ReactioNs). UNICORN, which solves full Navier-Stokes equations, has evolved over a 6-year period and is perhaps one of the most thoroughly evaluated codes of its kind. It evolved hand-in-hand with experiments that have been conducted to test its ability to predict ignition, extinction, and the dynamic characteristics of diffusion and premixed flames of hydrogen, methane, and propane fuels and that are stabilized in different ways. This paper also describes how UNICORN has been used, in conjunction with experiments, to provide new insights into combusting flows. Also, predictions of unobserved phenomena that were later confirmed by experiments are described. This paper demonstrates that the judicious use of a well-validated simulation in conjunction with laser based diagnostics is an effective way of understanding complex combusting flows.

Keywords: vortices, visualization, flames, combustion, laser diagnostics, turbulence.

1. Introduction

Studies of jet diffusion flames are important in understanding combustion phenomena, developing theories of combusting processes, and developing and evaluating design codes for practical combustion systems. Because of this, jet flames have been actively investigated since the classic works of Hottel et al. (1949). Considerable data on statistical quantities such as time-averaged and root mean squared (rms) values of velocity, temperature, and species concentrations have been obtained with single point measurement techniques. These data have formed the bases for understanding many of the processes occurring in jet diffusion flames. However, such understanding has limited applications for engineering problems because of the time-averaged description of the underlying unsteady combustion processes. In many cases, the mean and fluctuating quantities can mask the physics and chemistry that are germane to an understanding of the fundamental processes that give rise to the statistical results. This is particularly true for laminar and near-transitional jet flames in which the large-scale, low-frequency (0-40 Hz), organized, and absolutely unstable buoyancy-induced vortices on the air side of the flame and medium-frequency (100-1000 Hz), Kelvin-Helmholtz-type vortex structures on the fuel side of the flame dominate the flame characteristics. For example, high-speed visualizations of a buoyant jet diffusion flame have revealed that the flame surface is actually wrinkled as a result of the interaction of vortices, while time-averaged visualizations indicate a smooth surface. To gain insight into these low- and medium-frequency dynamic processes, it is helpful—and, perhaps, essential—to think in terms of the time-dependent characteristics of jet flames.

Several numerical investigations made in the past for dynamic jet flames using conserved-scalar approach, global-chemistry and detailed chemistry models have revealed important aspects of combustion such as effect of

heat-release rate (Ellzey et al., 1989; Yamashita et al., 1990), role of buoyancy (Davis et al., 1991; Katta and Roquemore, 1993; Patnaik and Kailasanath, 1994), enhancement of soot formation (Kaplan et al., 1996), and Lewis-number effects (Katta et al., 1994a; Takagi and Xu, 1994 ; Takagi et al., 1996). However, most of these studies, involving finite-rate chemistry, are limited to hydrogen fuel as the kinetic models for this fuel are relatively simple. Because of the complex nature of the reaction mechanisms, flame calculations for hydrocarbon fuels are restricted to either steady-state problems or chemically lazy flames in which chemistry is not important. Simulation of dynamic hydrocarbon flames with sufficiently accurate models for physical and chemical processes is required for understanding ignition, blow-out, instabilities, and emissions.

The authors have been developing a time-accurate CFDC (computational Fluid Dynamics with Chemistry) code (Katta et al., 1994a, 1994b, 1994c) known as UNICORN (UNsteady Ignition and COmbustion with ReactioNs) for the past six years. UNICORN is continuing to be developed as a research tool to better understand the dynamic characteristics of flames and as a future design tool for combustion systems. From its conception, the development of UNICORN has been strongly coupled with experiments that are designed: to evaluate the chemistry and transport models used in the code and to challenge its ability to predict complex dynamic characteristics of combusting flows. Because of the strong coupling with experiments, UNICORN is perhaps one of the most thoroughly evaluated Navier-Stokes based codes that have been developed. Visualizations have been used extensively in the development of UNICORN and in providing insights into the different combusting flows that have been studied. A simple view of the approach used to develop UNICORN is illustrated by the flame visualization in Fig. 1. The idea was to start the development of UNICORN by trying to predict the steady and dynamic characteristics of simple laminar like flames such as illustrated in Fig. 1(a), and then progress in a methodical way to the more complex flames illustrated in Figs. 1(b) and 1(c). This approach has proven to be extremely useful in systematically identifying and correcting deficiencies in the models used in UNICORN. It has also been demonstrated the power of using computations and experiments in concert to better understand both diffusion and premixed combustion flows. Indeed, UNICORN has evolved to the point where it has correctly predicted unknown combustion phenomena that were later confirmed experimentally. This paper illustrates the role of visualizations in the development of UNICORN and describes some of the insights into combustion processes that have resulted from the combined use of experimental and computational visualization methods.
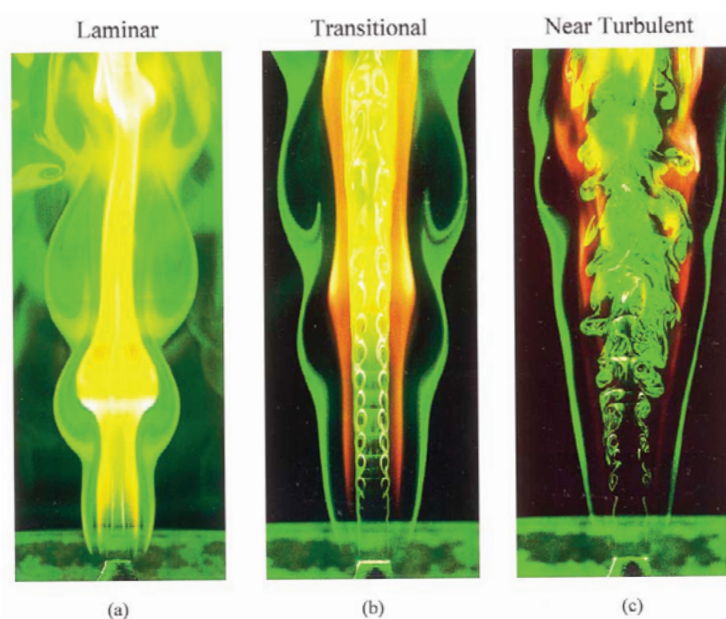

Fig. 1. Vertically mounted jet diffusion flame for different jet velocity conditions: (a) low-speed, laminar flame; (b) medium-speed, transitional flame; (c) high-speed, turbulent flame.

2. Model Description

UNICORN is a time-dependent, axisymmetric mathematical model that solves for axial- and radial-momentum equations, continuity, and enthalpy- and species-conservation equations to simulate a variety of dynamic jet flames. The governing equations, written in the cylindrical-coordinate system, are as follows:

$$\frac{\partial \rho}{\partial t} + \frac{\partial \rho u}{\partial z} + \frac{1}{r}\frac{\partial (r\rho v)}{\partial r} = 0 \tag{1}$$

and

$$\frac{\partial (\rho \Phi)}{\partial t} + \frac{\partial (\rho u \Phi)}{\partial z} + \frac{1}{r}\frac{\partial (r\rho v \Phi)}{\partial r} = \frac{\partial}{\partial z}\left[\Gamma^{\Phi}\frac{\partial \Phi}{\partial z}\right] + \frac{1}{r}\frac{\partial}{\partial r}\left[r\Gamma^{\Phi}\frac{\partial \Phi}{\partial r}\right] + S^{\Phi} \tag{2}$$

Table 1. Transport coefficients and source terms appearing in governing equations.

Φ	Γ^{Φ}	S^{Φ}
u	μ	$-\frac{\partial p}{\partial z} + (\rho_0 - \rho)\mathsf{g} + \frac{\partial}{\partial z}\left(\mu \frac{\partial u}{\partial z}\right) + \frac{\partial}{\partial r}\left(\mu \frac{\partial v}{\partial z}\right) + \frac{\mu}{r}\frac{\partial v}{\partial z}$ $-\frac{2}{3}\left\{\frac{\partial}{\partial z}\left(\mu \frac{\partial u}{\partial z}\right) + \frac{\partial}{\partial z}\left(\mu \frac{\partial v}{\partial r}\right)\right\} + \frac{\partial}{\partial z}\left(\mu \frac{v}{r}\right)$
v	μ	$-\frac{\partial p}{\partial r} + \frac{\partial}{\partial z}\left(\mu \frac{\partial u}{\partial r}\right) + \frac{\partial}{\partial r}\left(\mu \frac{\partial v}{\partial r}\right) + \frac{\mu}{r}\frac{\partial v}{\partial r} - 2\mu \frac{v}{r^2}$ $-\frac{2}{3}\left\{\frac{\partial}{\partial r}\left(\mu \frac{\partial u}{\partial z}\right) + \frac{\partial}{\partial z}\left(\mu \frac{\partial v}{\partial z}\right)\right\} + \frac{\partial}{\partial r}\left(\mu \frac{v}{r}\right)$
Y_i $_{(i=1-N_s-1)}$	ρD_{im}	$\dot{\omega}_i$
H	$\frac{\lambda}{c_p}$	$\nabla\left[\frac{\lambda}{C_p}\sum_1^{N_s}\left\{(Le^{-1}-1)H_i\nabla Y_i\right\}\right] - \sum_1^{N_s}\left(h_{f_i}^0 \dot{\omega}_i\right)$

Here ρ represents density; u and v are the axial and radial components of the velocity vector, respectively; and p is pressure. The general form of Eq. 2 represents the momentum, the species, or the energy-conservation equation, depending on the variable used in place of Φ. In Table 1, the transport coefficients Γ^{Φ} and the source terms S^{Φ} that appear in the governing equations are given. The body-force term due to the gravitational field is included in the axial-momentum equation. Here μ, λ, and c_p are the viscosity, thermal conductivity, and specific heat of the mixture, respectively; Y_i is the mass fraction; H_i is the enthalpy; $h_{f_i}^0$ is the heat of formation at standard state (temperature T_0); and ω_i is the mass-production rate of the ith species; ρ_0 is the density of air; and g is the gravitational acceleration. The transport property D_{im} is the effective diffusion coefficient of the ith species, which is calculated from the binary diffusion coefficients between that species and the other individual species. Finally, Le_i is the Lewis number of the ith species, which is defined as

$$Le_i \equiv \frac{\lambda}{\rho D_{im} c_p}. \tag{3}$$

The set of expressions given by Eqs. 1 and 2 can be completed using the global-species-conservation equation

$$Y_{N_s} = 1.0 - \sum_i^{N_s-1} Y_i \tag{4}$$

and the state equation

$$p = \rho T \quad_0 \sum_1^{N}\left(\frac{Y_i}{M_i}\right) \tag{5}$$

where R_0 is the universal gas constant; T is the temperature; and Y_i and M_i are the mass fraction and molecular weight of the ith species, respectively. While density is obtained by solving the state Eq. 5, the pressure field at every time step is determined from pressure Poisson equations. Even though the governing equations are solved in an uncoupled manner, the species-conservation equations are coupled through the source terms during the solution process to improve the stability of the algorithm. Such coupling is essential in finite-rate-chemistry calculations since the high-reaction-rate terms make the species-conservation equations quite stiff. Temperature- and species-dependent thermodynamic and transport properties are used in this formulation.

The governing equations for u and v momentum are integrated using an implicit QUICKEST (Quadratic Upstream Interpolation for Convective Kinematics with Estimated Streaming Terms) numerical scheme (Katta et al., 1994b; Leonard, 1979), which is third-order accurate in both space and time and has a very low numerical-diffusion error. On the other hand, the finite-difference forms of the species and enthalpy equations are obtained using the hybrid scheme (Spalding, 1972) with upwind and central differencing. An orthogonal, staggered-grid system with rapidly expanding cell sizes in both the z and the r directions is utilized for discretizing the governing equations. After rearrangement of terms, the finite-difference form of the governing equation for the variable Φ at a grid point P can be written as an algebraic equation as follows:

$$A_P\Phi_P^{N+1} + A_{z^{++}}\Phi_{z^{++}}^{N+1} + A_{z^+}\Phi_{z^+}^{N+1} + A_{z^-}\Phi_{z^-}^{N+1} + A_{z^{--}}\Phi_{z^{--}}^{N+1} + A_{r^{++}}\Phi_{r^{++}}^{N+1} + A_{r^+}\Phi_{r^+}^{N+1}$$
$$+ A_{r^-}\Phi_{r^-}^{N+1} + A_{r^{--}}\Phi_{r^{--}}^{N+1} = S_P^{\Phi} + \Delta t.\rho_P\Phi_P^N \qquad (6)$$

The time increment, Δt, is determined from the stability constraint and maintained as a constant during the entire calculation. The superscripts N and $N+1$ represent the known variables at the Nth time step and the unknown variables at the $(N+1)^{th}$ time step, respectively; the subscripts z^+ and z^- indicate the values at the grid points immediately adjacent to point P in the positive and negative z-directions, respectively. Similarly, the subscripts z^{++} and z^{--} represent the values at two grid points from P in the respective directions. The coefficients A and the terms on the right-hand side of the above equations are calculated from the known flow variables at the Nth time step. The above equations for $N+2$ variables are solved individually using an iterative ADI (Alternative Direction Implicit) technique. The pressure field, at every time step, is accurately calculated by simultaneously solving the system of algebraic pressure Poisson equations at all grid points using the LU (Lower-Upper) decomposition technique.

The enthalpies of all the species are calculated from the polynomial curve fits developed for the temperature range 300-5000K. Physical properties such as viscosity, thermal conductivity, and the binary molecular diffusion coefficients of the species are calculated using molecular dynamics. Mixture viscosity and thermal conductivity are then estimated using the Wilke and the Kee expressions (Hirschfelder, 1954), respectively. Molecular diffusion is assumed to be of the binary type, and the diffusion velocity of a species is calculated according to Fick's law and using the effective-diffusion coefficient (Williams, 1985) of that species. The Lennard Jones potentials, the effective temperatures, and the coefficients for the enthalpy polynomials for each species are obtained from the CHEMKIN libraries.

3. Results and Discussion

Many chemistry models have been used in the evolution of UNICORN, starting with a one step global model for hydrocarbon fuels and progressing to complete chemistry for hydrogen to near complete chemistry for propane. These models were used in studying different aspects of steady and unsteady flames. Some of these results are discussed in the following sections.

3.1 Flame-base Structure

Predictions of the attachment region of jet flames are a significant challenge for CFD based codes. The reason is that near the stability limit of these flames, the calculations are strongly dependent on the accuracy of various mathematical models incorporated into the code. Even though, the exact mechanisms that govern the stability of a diffusion flame are less understood, it is generally believed that flow field, chemistry and heat and mass transfer are important for the simulation of flames near the stability limit. UNICORN has been used to investigate the stability phenomenon by simulating three methane jet diffusion flames that were experimentally found to be near the stability limits (Takahashi and Schmoll, 1991). The photographs of the three flames taken by seeding the flow with PIV particles are shown in left halves of Figs. 2(a), 2(b), and 2(c), respectively. The blue region in these

photographs represents the luminous flame, which, in general, will be located within the high-temperature region. The inner diameter and wall thickness of the fuel tube are 9.5 and 0.45 mm, respectively. The flow conditions and the stability statuses for the three flames are listed in Table 2.
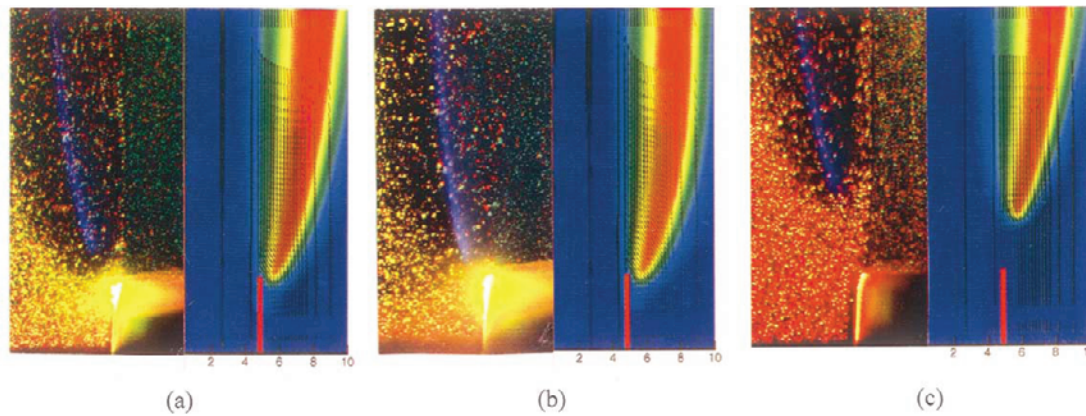

Fig. 2. Methane jet diffusion flames operating close to stability limits: (a) higher fuel jet and lower annular air velocities– attached flame; (b) medium fuel and air jets – attached flame; (c) lower fuel jet and higher annular air velocities– separated flame.

Table 2. Flow conditions used for the flame stability studies.

Flame No.	U_j (m/s)	U_a (m/s)	Stability
1	11.5	0.19	attached
2	6.9	0.36	attached
3	1.7	0.72	separated

Calculations for the three methane flames in Table 1 were made using Peters 17-species and 52-reaction model (Peters, 1993). The fully developed pipe flow and boundary-layer velocity profiles were used inside and outside the fuel tube, respectively. Results in the form of velocity vectors superimposed over the temperature field are shown on the right halves of the quantitative visualizations in Figs. 2(a), 2(b), and 2(c). A comparison of experimental and simulated flame visualizations in Fig. 2 suggest that the code is able to reproduce the stability phenomenon of diffusion flames. Calculations have resulted in attached flames for the cases 1 and 2 and a 3-mm separated flame for case 3. After obtaining this general agreement between experiments and calculations, the flow and chemistry data associated with the simulations is further analyzed to understand the mechanisms responsible for stabilizing diffusion flames and the results are published recently (Takahashi and Katta, 1997; Takahashi et al., 1998).

3.2 Unsteady Laminar Flames

UNICORN was developed for the purpose of accurately predicting the dynamics characteristic of unsteady combustion flows. The ability of UNICORN to predict unsteady combustion processes has been tested by conducting experimental/numerical investigations on various dynamic flames. Extensive experimental studies have been performed on buoyant, laminar jet flames that tend to oscillate at a stable frequency. An example of such flames is the hydrogen/air buoyant jet diffusion flame studied by Vilimpoc and Goss (1988). The time-accuracy of results obtained with UNICORN was investigated by simulating this flame. The fuel used was a mixture of hydrogen and nitrogen in a volumetric ratio of 3.5 to 1. The flame was stabilized on a contoured nozzle having an exit diameter of 10 mm. The fuel jet was mounted vertically and had a mass averaged exit velocity of 3.55 m/s. The flame was surrounded by a 150-mm-diameter co-annular air jet having a velocity of 35 cm/s which helped to shield the central jet flame from room-air disturbances. An instantaneous image of the experimental flame visualized by the Reactive-Mie-Scattering technique (Roquemore et al., 1989) is shown in Fig. 3(a). At this low jet velocity, the shear layer is laminar in nature, and no shear-layer instabilities have developed. Three outside large-scale structures are clearly visible, even though the third one at the top is somewhat smeared by the room air.
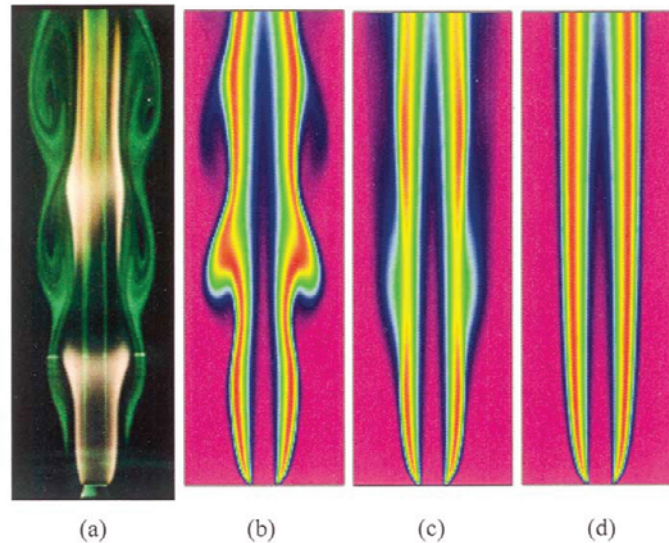
Fig. 3. Comparison of experimental and computed hydrogen/air flames for fuel-jet velocity of 3.26 m/s: (a) Reactive-Mie-Scattering image of experimental flame; (b) instantaneous temperature contours of computed flame; (c) iso-temperature contours obtained from time-averaged flame; (d) iso-temperature contours of steady-state flame.

Calculations were performed using a chemical-kinetics model consists of 8 species and 26 reactions (Katta et al., 1994a). An instantaneous iso-temperature color visualization of the computed flame is shown in Fig. 3(b) at a phase very near that of the experimental image in Fig. 3(a). It should be pointed out that no artificial perturbations were introduced to generate these buoyancy-driven structures. Once a vortex is developed it rolls along the flame surface while it is convected downstream. During this process, the vortex interacts strongly with the flame, making the flame surface bulge and squeeze. This motion is simulated by the time-dependent calculations, as observed in animations of the dynamic characteristics of the flame. Freezing of the flame motion, as in Figs. 3(a) and 3(b), shows that the bulging and squeezing of the experimental and computed flame surfaces occur at about the same heights. Excellent agreement was obtained between the calculated and measured flame-flicker frequency. At 80 mm above the nozzle, a 14.8-Hz frequency was obtained from the computed temperature fluctuations, while the frequency was observed to be ~15 Hz in the experiments.

Time averaged data and steady state calculations can provide misleading information about unsteady flames. This is illustrated in the time-average visualization of several instantaneous temperature contours shown in Fig. 3(c). In the averaged view, the second and third buoyant structures have disappeared, but the first structure is still evident as a locally diffused flame. Since the mean temperature reflects the time the flame spends at a given location, the presence of the first bulge indicates that the flame spends considerable time in the bulged position at an axial location between 50 and 100 mm. The isotherms in the interior of the jet ($r < 10$ mm) are only moderately affected by the dynamic motion of the outer structures, as evidenced by the similarity of the instantaneous [Fig. 3(b)] and averaged [Fig. 3(c)] isotherms. To illustrate the importance of simulating the dynamic flames using unsteady CFD code, calculations were also performed for the same flame using the steady-state option of UNICORN. Solution for this case converged to a flame having perfectly smooth surface. The iso-temperature visualization of the resulted flame is shown in Fig. 3(d); which does not resemble either the instantaneous flame [Fig. 3(b)] or time-averaged flame [Fig. 3(c)].

The computed time evolution of temperature as the large outer structures are convected past a fixed radial line 80 mm above the nozzle tip is visualized in Fig. 4. The data shown at $\tau = 150$ ms represent the temperature recorded 150 ms prior to that shown at 0 ms. Bulging and squeezing of the flame due to the convective motion of the outer vortices cause the periodic oscillation in the flame surface and create the elliptical-shaped islands of relatively cold fuel (< 1500K) near the centerline of the jet. The temperature evolution of the experimental flame at the same height ($z = 80$ mm) obtained using Thin-Filament-Pyrometry technique (Goss et al., 1989) compares well with the predictions. The period of oscillation measured from this plot (~65 ms) matches that obtained from the frequency data obtained from experiments.
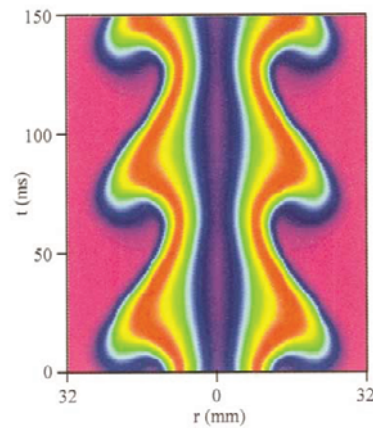
Fig. 4. Predicted temperature evolution of the flame in Fig. 3 at 80 mm above nozzle.
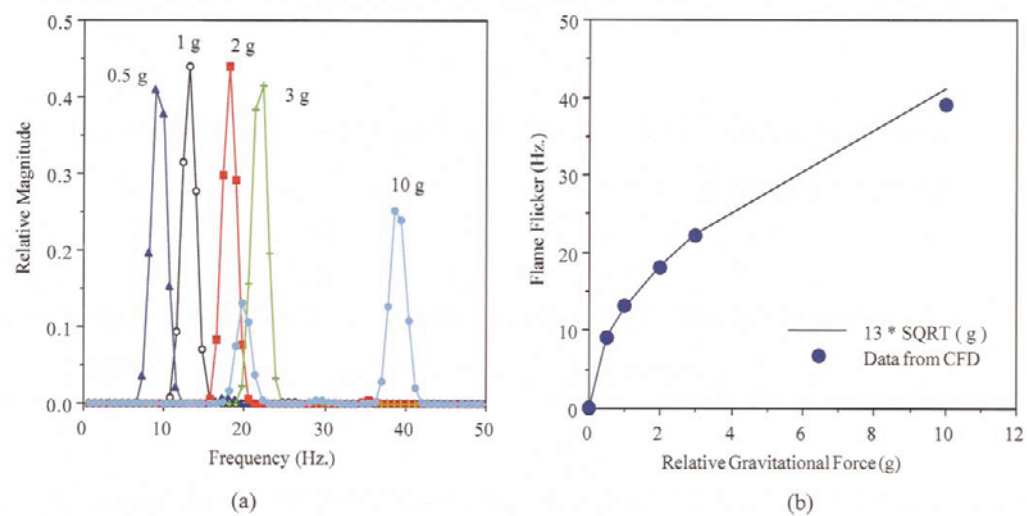

Fig. 5. (a) Frequency spectra obtained from temperature for different gravitational forces; (b) correlation between flicker frequency and gravitational force.

One of the powerful features of simulations is that one can systematically vary parameters that cannot be easily varied in experiments. This is illustrated by a study of the flame similar to that in Fig. 3. A lower air flow of 0.2 m/s is used in this numerical experiment. The gravitational force was varied to determine the effects of buoyancy on the outer structures. Calculations were made with 1/2 g*, 1 g*, 2g*, 3g* and 10 g*, where g* is the earth's gravitational acceleration. As expected, the diameter of the flame decreases and the frequency of oscillation increases with g. The flame oscillation is found to be very periodic up to 3 g*. At 10 g* the oscillations appear to be a combination of two oscillations having different frequencies and magnitudes. Frequency spectra from the temperature fluctuations are obtained using FFT (Fast Fourier Transform) and are shown in Fig. 5(a). The peaks are somewhat broad because of the limited number of samples stored. Nevertheless, each spectrum except that of 10g* case has a single peak, indicating the periodicity of the flow. For the normal-gravity (1 g*) case, the frequency for the outer structures is 12.8 Hz. The frequency spectrum for the 10 g* case has two distinct peaks. The one at 38 Hz corresponds to the fundamental frequency, and the subharmonic of this (19 Hz.) appears as the second peak. The variation of the flame-flickering frequency with respect to gravitational force is plotted in Fig. 5(b). The data points are well fitted with the following equation:

$$\text{Flickering Frequency } = f * \sqrt{\frac{g}{g^*}}$$

where f^* represents the flickering frequency for the gravitational acceleration g* of the earth. Additional calculations at a very low g (= 0.05g*) also yielded a frequency that is falling right on top of the curve-fit given by

the above equation. The predicted square-root dependence of the frequency on gravitational acceleration is supported by the recent microgravity experiments of Bahadori et al. (1996).

3.3 Unsteady Transitional Flames

Calculations were made for a transitional hydrogen flame having a fuel jet velocity of 7.64 m/s. The volumetric ratio between the hydrogen and nitrogen in this case was 3.44 to 1. A Reactive-Mie-Scattering image of an instantaneous flame is shown in Fig. 6(a). This flame is highly symmetric, even up to a height of 250 mm (25 diameters) and has well-organized structures both outside and inside the flame surface. As the inner vortices move downstream, they are squeezed radially and elongated axially but still retain their symmetry.
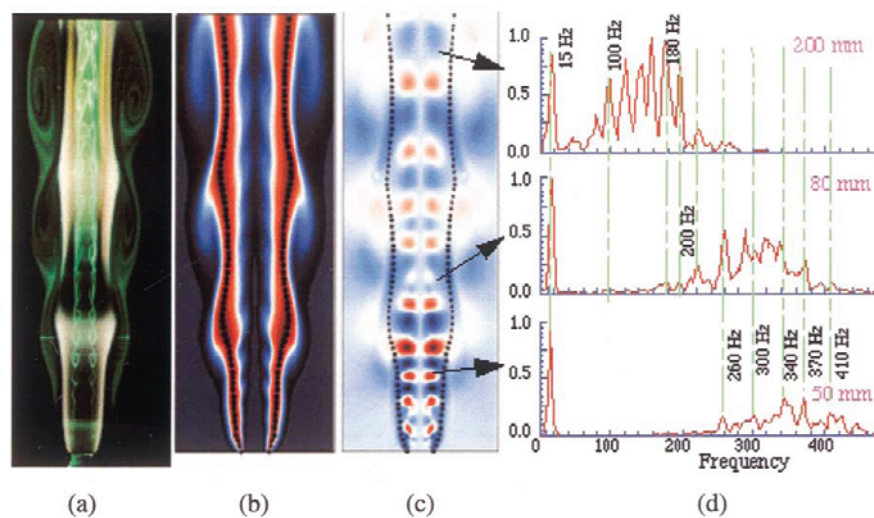

Fig. 6. Visualization of large-scale outer and small-scale inner vortices of 7.64-m/s hydrogen/air flame: (a) experimental flame obtained with Reactive-Mie-Scattering technique; (b) instantaneous iso-temperature contours of computed flame; (c) instantaneous iso-radial velocity map; (d) frequency spectra obtained from temperature data recorded within shear layer at different axial locations.

The computed results in the form of iso-temperature and iso-radial-velocity plots are shown in Figs. 6(b) and 6(c), respectively. In order to generate and sustain the shear-layer instabilities in the calculated flame, random disturbances were introduced at the exit of the fuel-jet. First, a few millimeters above the nozzle, but within the shear layer, a circular zone having a radius of three grid spacings was chosen. At all grid points within this zone, random disturbances of 1% magnitude were introduced to the local axial-velocity component. In the isotherms plot [Fig. 6(b)] and iso-axial velocity plots, the inner vortices appear as wavy lines. On the other hand, these vortices are more evident in the iso-radial-velocity contours of Fig. 6(c). Here, red and blue colors represent positive (outward) and negative (inward) radial velocities, respectively.

A comparison of the calculated flame in Figs. 6(b) and 6(c) with the experimental flame in Fig. 6(a) shows that the simulation provides a good prediction of the structural features of the inner vortices. The numerical model was able to predict the flame-surface location with reasonable accuracy up to a height of ~200 mm above the nozzle. For example, the computed flame diameters at the first three flame bulges from the nozzle are 37, 41, and 42 mm, respectively, as compared to 32, 41, and 41 mm measured from the experimental image. Also, the frequency of the computed inner vortices, as noted by the number of vortices per unit length, is about the same as that in the experiments. The simulation also correctly predicts the unusual spatial development of the vortices as they are convected downstream. Note that in the experiment, Fig. 6(a), the vortices in the shear layer of the jet do not grow radially as they do in cold jets. Instead, the vortices grow axially and become elongated as they are convected downstream. The computed inner vortices in Figs. 6(c) exhibit these same characteristics.

Figure 6(d) shows frequency spectra obtained from temperature data collected at a radial location of 5 mm within the shear-layer at different axial distances from the nozzle exit. The data, stored from 10,000 time-steps, covered a real time of 0.75 s. The calculated spectra compare favorably with those measured by Lee (1992) in a 10-mm-diameter jet diffusion flame. The fuel was hydrogen and nitrogen with a mixture ratio of 3.5 to 1. The exit

velocity at the jet was 7.8 m/s (Lee, 1992). Lee used Fourier transforms to obtain the spectrum from time and spatially resolved temperature measurements using Thin Filament Pyrometry at several heights in the flame. The spectral peaks at a height of 50 mm were compared with those shown in Fig. 6(d) at a height of 50 mm. The measured peak frequency was ~340 Hz, with smaller peaks at ~380, 480, 300, 240, and 15.6 Hz. This compares favorably with the calculated peak frequency of 340 Hz and smaller peaks at ~370, 410, 300, 260, and 15 Hz. Spectra measured at downstream locations showed the same trends as those in Fig. 6(d). That is, the peak frequencies decreased with height. A similar shift from high to low frequency with height in the flame was also observed by Yule et al. (1981) for a 6-m/s methane flame having well-organized inner vortices. From this limited analysis, the simulation appears to predict the spectrum reasonably well, which suggests that it has captured the essential physics of the problem.

Both the inner and outer vortices of the flame shown in Fig. 6 seem to interact with the flame surface by locally squeezing or expanding. During this process the flame temperature could change. However, the degree to which the vortex-flame interaction alters the flame temperature is dependent on the local Lewis number. Similarly, this interaction may also modify the species concentration as a result of the variations in species diffusion coefficients. The interaction of the inner and outer vortices with the flame was studied by plotting radial distribution of temperature at an axial location of 120 mm (Fig. 7). Scattered instantaneous values were obtained over a period of 0.4 s. The average profile is shown by solid line. From the visualization of the temperature-evolution in Fig. 7(a) at this axial location, it was observed that the flame surface oscillates radially between r = 13 and 17 mm. As mentioned previously, the outer vortices are mainly responsible for this oscillation.
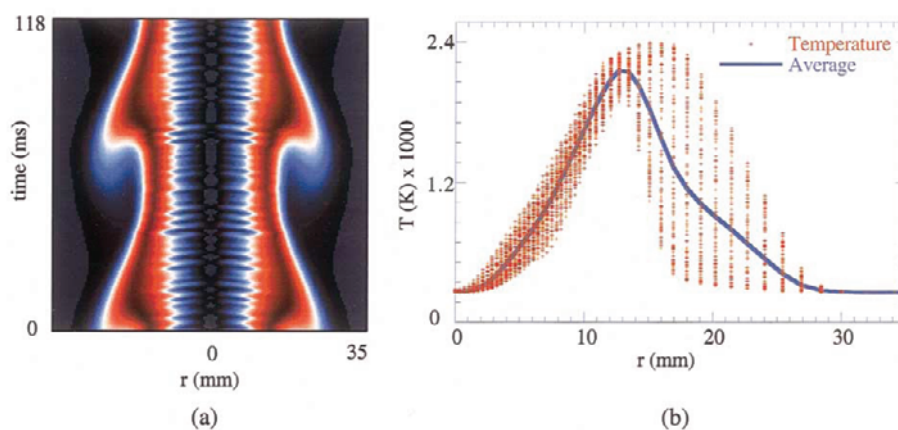

Fig. 7. (a) Predicted temperature evolution; (b) scatter plot of temperature fluctuations of the flame in Fig. 6 at a height of 80 mm above nozzle.

The scatter plot of instantaneous temperatures [Fig. 7(b)] indicates that the flame temperature reaches a maximum value when it is pushed outward radially, i.e., at r = 17 mm. As the flame moves radially inward, the peak temperature gradually decreases; however, a maximum in average temperature occurs near the radially most inward location of the flame. With reference to Fig. 7(a) and the scatter plot in Fig. 7(a), it should be noted that the outer vortices cause more temperature fluctuations outside the flame surface than inside; therefore, the average temperature is lower at *r* > 13 mm.

3.4 Vortex-flame Interactions

At this point, UNICORN has been thoroughly evaluated using steady, unsteady, and transitional flames. The logical next step in its development is to proceed to turbulent combusting flows. This means adding a subgrid model and three-dimensionality to UNICORN. This is relatively simple process as far as code development goes, however; the price comes from extremely long computational times. We viewed the long computational times as more of an impediment instead of an advancement in the development process. Thus, we started thinking about how we could approach the turbulent problem without making a large sacrifice in computational time. Our approach is to eliminate the statistical nature of turbulence that makes it difficult to study and investigate individual turbulent events that could be created repetitively in the laboratory and studied with a two-dimensional code.

A turbulent flame can be thought of as an ensemble of different individual vortex-flame interactions. A

flame is considered to be fully turbulent, according to Hottel and Hawthorne (1949), when its entire surface area becomes a flame brush, i.e., highly wrinkled, bumpy, and rough. The wrinkles and bumps in the flame are the localized protrusions of the flame surface that result from the interaction of the three-dimensional fluid elements with the reaction zone. Photographs (Fig. 8) taken with high-speed cameras indicate that these interacting fluid elements (insert in Fig. 8) in a turbulent flame are often associated with vortices of different sizes, shapes, and strengths. As seen in the last section there are many interesting, yet not well understood, processes associated with vortex-flame interactions. In this section, we describe the results of computational and experimental studies of vortex-flame interactions starting with naturally developing vortices in buoyant diffusion flames and progressing to driven vortices.
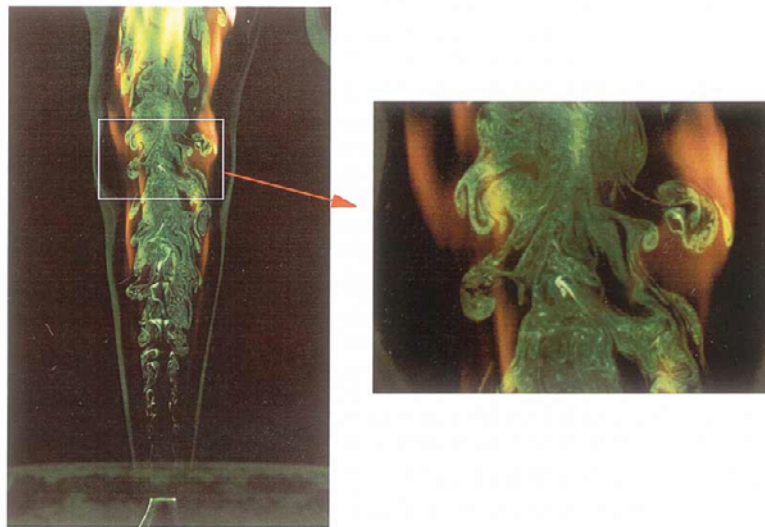

Fig. 8. Near-turbulent jet diffusion flame showing the random vortex-flame-interaction events. Blowup of such an event is shown in the insert.

(1) Naturally Developing Vortices

Studies on various low-speed jet diffusion flames show that the buoyancy generated large-scale vortical structures interact with the flame surface as they are convected downstream. These highly periodic flames provide data for understanding chemical and fluid-dynamic aspects of the vortex interactions with a laminar flame. Recent numerical studies (Katta et al., 1994a; Katta and Roquemore, 1995) on a low-speed buoyant H_2/air jet diffusion flame using UNICORN and finite-rate chemistry with NO-formation reactions have predicted that the local temperature and concentration of NO increase in the compressed regions and decrease in the stretched regions of the flame. Laminar-flamelet theory (Peters and Williams, 1983) suggests that when a diffusion flame is stretched (as in a vortex-flame interaction) the flame temperature decreases due to the increased reactant fluxes. Furthermore, the reduced Damkohler number (ratio of residence time to reaction time), might explain the predicted changes in the stretched regions of the flame, however, it could not explain the temperature changes in the compressed regions of the vortex-flame interaction. The explanation of the change in temperature in the stretched and compressed regions of a flame, as described in detail in Katta and Roquemore (1995), is based on the non-unity value of the local Lewis number and curvature effects. This explanation is qualitatively consistent with the studies of Law (1984). To verify these predictions, two experimental studies have been undertaken, one conducted by Carter et al. (1995) and a second conducted by Grisch et al. (1996). In both experiments, phase-locked measurements of temperature and NO concentrations were made as an outer vortex interacted with a low-speed hydrogen/air jet diffusion flame.

Measured and computed variations in temperature and molar concentration of OH and NO across the flame with time at an axial distance of 80 mm are plotted in Figs. 9(a), 9(b), and 9(c), respectively. Data at elapsed time τ represent the flame as observed at τ ms prior to zero. Measurements are visualized on the left side of each figure and computed results are visualized on the right side. Temperatures were measured using the Thin-Filament-Pyrometry technique (Goss et al., 1989) and OH and NO concentrations were obtained using Laser Induced Fluorescence (Carter et al., 1995). Measurements shown in Fig. 9(a) confirm the predicted increase in temperature

in the compressed region and decrease in temperature in the stretched region. The species OH is confined to a narrow zone and is mostly on the air-side of the flame. Its concentration decreases as the flame is pulled radially outward. Measurements shown in Fig. 9(c) also confirm that a large fraction of the NO is produced during the vortex-flame interaction and on the air-side of the high-temperature surface. Entrainment of NO into the air-side vortex indicates the longevity of the NO molecules. In contrast to the behavior of OH, NO production becomes maximum when the flame is bulging outward (compressed).
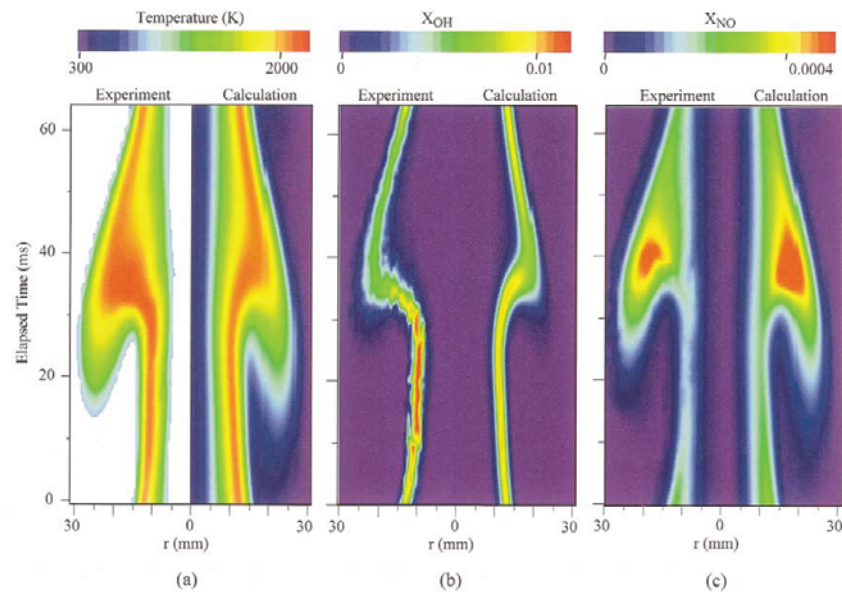

Fig. 9. Evolution of (a) temperature, (b) OH concentration, and (c) NO concentration of dynamic flame shown in Fig. 3 at axial location of 80 mm from nozzle exit. Data at any given elapsed time, *t*, represents that the observer might have seen *t* ms prior to 0. Contour table for each plot is given at the top. In each figure measurements are shown on the left and predictions on the right.

In the second experiment, Grisch et al. (1996) have measured temperatures and NO-concentrations using CARS and Degenerative-Four-Wave-Mixing techniques, respectively. Measurements were made on a similar flame that had a slightly smaller fuel flow rate than that shown in Fig. 9. Measurements were made at the fixed axial ($z = 135$ mm) and radial locations ($r = 6.5$ and 16.5 mm) and the data are plotted (symbols) along with the corresponding computed values (solid lines) in Fig 10. In this plot, the molar concentration of NO in the experimental and computed flames are compared using relative units. Both the calculations and experiments show that at radial locations away from the flame surface [Fig. 10(a)] the periodic variations in NO concentration follow closely that of temperature. However, near the flame surface [Fig. 10(b)] the concentration of NO is much higher in the compressed region compared to that in the stretched region. The two peaks in the temperature profile at times 77 and 92 ms represent the stretched and compressed flamelets, respectively. As observed in the previous experimental (Vilimpoc and Goss, 1988) and numerical (Katta and Roquemore, 1995) studies, the temperature of the compressed flamelet is higher than that of the stretched flamelet and it was attributed by Katta et al. (1994a) to the non-unity Lewis number of the local gas mixture. Measurements seem to exhibit larger variation in temperatures of the stretched and compressed flamelets than was predicted. However, calculated data at a radial location slightly different from that used in Fig. 10(b) show a temperature difference of ~100 K. Thus, the agreement between the measured and computed data at both radial locations [Figs. 10(a) and 10(b)] for both temperature and NO concentration is considered to be very good. This comparison confirms the fact that temperature and NO concentration indeed increase with the flame compression; with the NO concentration being affected more significantly.
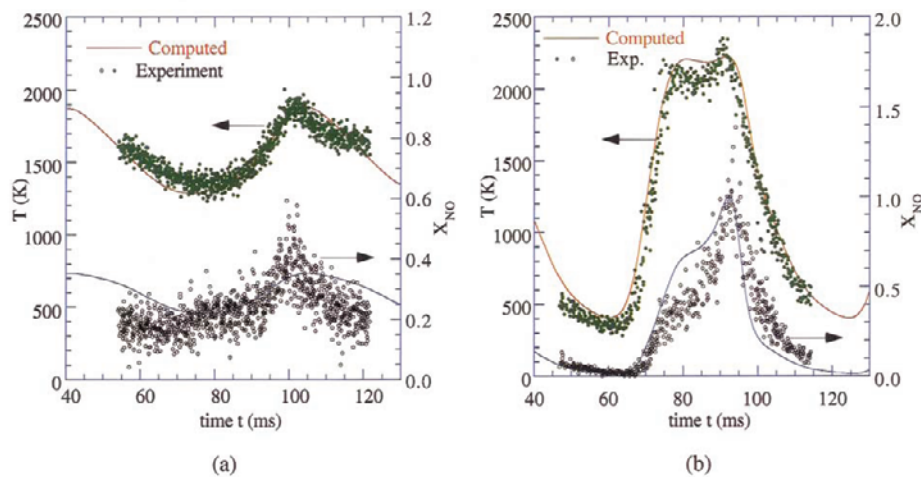
Fig. 10. Predicted and measured temperature and NO-concentration fluctuations obtained at axial distance of 135 mm and at radial locations of (a) 6.5 and (b) 26.5 mm in a buoyant hydrogen/air jet diffusion flame.

(2) Driven Vortices

Studies involving vortices that are formed and interact naturally with the flame surface provide valuable insights into vortex-flame interactions, however, there are also some major limitations associated with such studies as the size and strength of the vortices cannot be readily changed. Typically, the vortices, that develop in buoyant jet flames, range in size of several centimeters for laboratory flame to several meters in large fires. Only the larger vortices produce sufficient stretch to cause local extinction. On the other hand, turbulent flames involve strong interactions between flames and vortices having sizes ranging from mm to several meters. Therefore, to understand vortex-flame interactions that could simulate those in turbulent flames, studies must be performed with various sizes of vortices. This can be achieved by externally driving a vortex and forcing it to interact with a flame in a controlled way.

Hsu et al. (1993) established a vortex inside a laminar jet diffusion flame fueled with methane by driving the fuel jet. The experimental setup consists of a central fuel nozzle and a coannular air duct with exit diameters of 10 and 152 mm, respectively. The fuel nozzle is connected to the speaker chamber by means of a long tapered tube. Fuel is pumped through the side ports of the speaker chamber. An audio speaker is mounted in this chamber in such a way that the hollow cone of the diaphragm is toward the nozzle exit. While a steady flow of fuel is maintained throughout the experiment, puffs of fuel are periodically ejected from the nozzle by driving the speaker with a pulse generator. The flame is shielded from room-air disturbances using a low-speed air flow in the coannular duct. This system permits precise control of the frequency, strength, and shape of the vortex that emerges from the fuel nozzle.

Phase-Locked RMS visualizations at 8, 10, 12 and 14 ms after firing the vortex are shown from left to right in upper half of Fig. 11. The vortex structures captured by the RMS visualizations can be recognized by their dark green-yellow appearance. These images are frozen by the 10-ns flash of the laser sheet passing through the center of the flame and thus, accurately represent the time and spatial evolution of the vortices. However, the flame image is the result of averaging by the film during the time the camera shutter is open, which is about 1 ms in this case. The apparent flame locations in Fig. 11 are marked by the yellow and blue colors in the photograph.

The vortex-flame interactions are evident in Fig. 11. At the 8-ms instant, a large vortex that rotates downward is observed. There is also a counter rotating "secondary" vortex on top of the large "primary" vortex but it is too small to be clearly observed. Two milliseconds later, however, the size of the "secondary" vortex became comparable to that of the "primary" vortex. It is clear that they form a pair of counter rotating vortex rings. Almost all of the outward radial motion of the vortices occurs between 0 and 10 ms. The vortex interaction with the flame produces a hole that occurs between 8 and 10 ms. Once the hole is formed and the vortex pair reaches its maximum radial location, it appears to rotate inward. This is observed for time-delays of 12 and 14 ms. The hole–which is clearly a ring, as noted by the dark band across the flame–remains open for a long period of time.
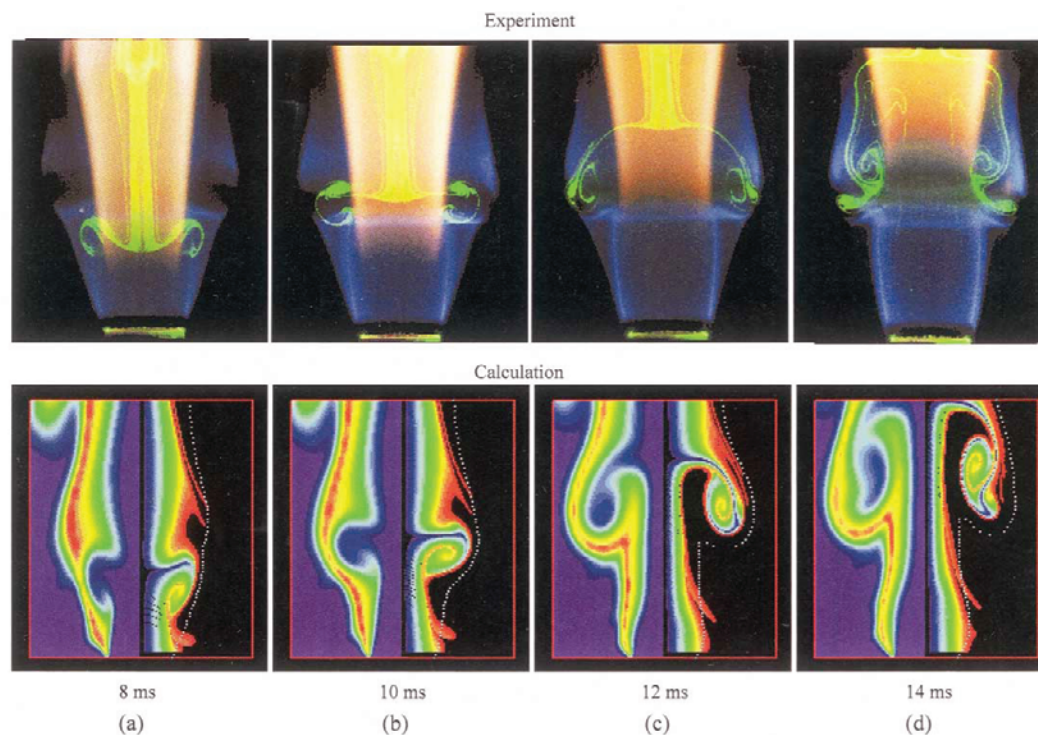
Fig. 11. Vortex-flame interaction in driven methane/air jet diffusion flame. Experimental images obtained using Reactive-Mie-Scattering technique are shown in the upper half. Green emission from TiO_2 particles represents instantaneous flowfield, and blue color represents time-averaged flame surface. Predictions made using global-chemistry model are shown in the lower half. Temperature is plotted on left and particle locations are plotted on right.

The results of the numerical simulations at approximately the same time-delays as those of the experiments of Fig. 11 are shown in the lower half of Fig. 11. Composite visualizations of isotherms (left) and color-coded particle tracings (right) are presented at each instant. Also shown in the figure are the predicted instantaneous stoichiometric mixture fraction locations, marked by the white dots outside the particle tracings. The numerical simulation reproduces the evolution of the primary vortex of the experiments using the particle tracking technique. The counter-rotating vortex ring is also evident in the simulation. The isotherm representation did not identify the vortex pair that is shown by particle tracings. In fact, the temperature field prediction seems to suggest the existence of a single vortex region. The numerical simulation appears to produce nearly the same time and spatial evolution of the ring vortex as observed in the experimental visualizations.

Note that the computed visualizations in Fig. 11 appear to capture the quenching process during the vortex-flame interaction just as observed in the experiments. However, the flame is not completely quenched since there is still a high temperature zone. It appears that the high temperature is thinned out by the vortex-flame interaction. Quenching normally results from a reduction in chemical reaction rate and hence a reduction in heat release rate. However, chemical quenching is not possible because infinitely fast global reaction chemistry was used in the calculations. The thinning of the flame zone with infinitely fast chemistry is an interesting phenomenon. A better understanding of the processes causing it could give additional insights into the quenching process. It is useful to examine how the flame thinning comes about in the calculations. The insights will come form visualizing the vortex-flame interaction in several different ways.

Figure 12 is a visualization of the computed vortex-flame interaction at a time when the flame is stretched thin. The left side of the visualization contains an iso-temperature color plot and the right side contains iso-concentration plots of fuel and oxygen fields separated by the peak-temperature surface (solid white dots). The instantaneous particle field is superimposed on the right-hand side image and the velocity field is superimposed on the left-hand side. Note that particle tracking provides a visualization that is very similar to the RMS visualizations shown in Fig. 11. The particle track and velocity vector visualizations in Fig. 12 show that the primary counter-rotating ring vortex has a high radial velocity in the region where the flame is being stretched. This is due to the

fuel being deflected as it approaches the flame zone. The fuel is deflected away from the flame zone because of the high viscosity barrier caused by the high temperature around the flame surface and the large density ratio between the entrained fluid and the flame. Since the deflected fuel is not transported into the flame, the flame thickness momentarily decrease even though infinitely fast chemistry is used in the simulation. The decrease in flame temperature is resulting from the coarseness of the mesh used. It should be noted that different ways of visualizing the flame thinning process provided the insights into the transport processes causing it. However, the question as to whether the real quenching process observed in Fig. 11 is due to the deflection of fuel from the flame or from finite rate chemistry has not been answered. To address the effects of finite rate chemistry calculations were performed using Peters' chemical kinetics (Peters, 1993). Details of these investigations are published else where (Katta et al., 1998b).
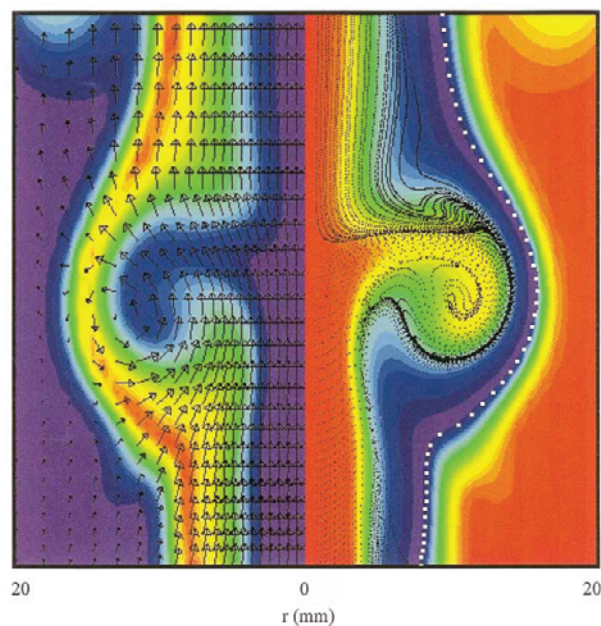

Fig. 12. Blowup of the vortex-flame interaction at an instant corresponding to Fig. 11(b). Temperature and velocity field are shown on the left-hand side. Fuel and oxygen concentrations and particle locations are shown on the right-hand side.

In previous sections, the results of combined numerical/experimental investigations have demonstrated the value of visualization in evaluating UNICORN and using it as a research tool to understand simple, dynamic flames. A long-range goal for UNICORN is that it will be used as a tool to aid in the design of practical combustion systems such as gas turbine combustors. Recently, UNICORN has been used for the prediction of complex flowfields in research combustors (Durbin et al., 1996; Katta and Roquemore, 1998a) and demonstrated the need for dynamic simulations in those combustors.

4. Summary

Accurate simulations employing detailed-chemical-kinetics models for different fuels are needed for understanding flame structure and various processes involved in unsteady flames. An axisymmetric, time-dependent CFDC (Computational Fluid Dynamics with Chemistry) code known as UNICORN has been developed over the past 6 years for the simulation of dynamic flames. During its development, experimental/numerical investigations have been performed on various flames to validate and establish the accuracy of the predictions. Both qualitative and quantitative visualizations have been used extensively for comparing the predictions with experimental data and in exploring the physics associated with the problems. Parametric studies have also been conducted to identify the factors that are important in these dynamic flames.

Calculations using UNICORN have been performed for unsteady laminar and transitional jet diffusion flames of hydrogen, methane and propane fuels. The predicted flame shapes and flow structures of periodically

oscillating flames, that result from an absolute buoyancy-induced instability, showed good correlation with the Reactive-Mie-Scattering images of the flames obtained in experiments. UNICORN predicted and it was later found experimentally that the temperature and hence, nitric oxide, in these buoyancy-dominated unsteady flames increase at certain phases of the vortex-flame interaction; a characteristic behavior of hydrogen and methane flames. Simulations for transitional flames having inner and outer vortices reveled that viscosity, volumetric expansion and body force due to buoyancy are responsible for the slower growth and longer coherence lengths for the inner vortices.

A combined experimental/numerical study was made for the vortex-flame interactions in a coflowing methane jet diffusion flame. A large toroidal vortex formed from the fuel puff and pushed the flame radially outward and created a hole on the flame surface. As the vortex convected downstream, re-ignition took place in the region of the hole and the flame returned to its unperturbed position. UNICORN has been used to investigate the vortex evolution, quenching and ignition processes associated with this vortex-flame interaction.

Acknowledgments

References

Bahadori, M. Y., Zhou, L., Stocker, D. P. and Hegde, U., "Measurements of Flame Flicker Under Different Gravitational Levels," Proceedings of the 1996 Fall Technical Meeting of the Eastern States Section of The Combustion Institute, Pittsburgh, PA, (1996), 451-454.

Carter, C. D., Goss, L. P., Hsu, K. Y., Katta, V. R. and Trump, D. D., Paper No. 080, Proceedings of the Combined Central States/Western States/Mexican National Sections Meeting of the Combustion Institute, April 23-26 (1995).

Davis, R. W., Moore, E. F., Roquemore, W. M., Chen, L.-D., Vilimpoc, V. and Goss, L. P., "Preliminary Results of a Numerical-Experimental Study of the Dynamic Structure of a Buoyant Jet Diffusion Flame," Combustion and Flame, 83, 3/4, (1991), 263-270.

Durbin, M. D., Vangsness, D., Ballal, D. and Katta, V. R., "Study of Flame Stability in a Step Swirl Combustor," Transactions of the ASME: Journal of Engineering for Gas Turbine and Power, 118, (1996), 308.

Ellzey, J. L., Laskey, K. J. and Oran, E. S., "Dynamics of an Unsteady Diffusion Flame: Effects of Heat Release Rate and Viscosity," in Dynamics of Deflagrations and Reactive Systems: Flames, A. L. Kahl, J. C. Leyer, A. A. Borisov, and W. A. Sirgnano, Eds., Vol. 131, Progress in Astronautics and Aeronautics, (1989), 179, American Institute of Aeronautics and Astronautics, Washington, D. C..

Goss, L. P., Vilimpoc, V., Sarka, B. and Lynn, W. F., "Thin-Filament Pyrometry: A Novel Thermometric Technique for Combusting Flows," ASME Trans., J. Eng. Gas Turbines Power, 111, (1989), 46.

Grisch, F., Attal-Tretout, B., Bouchardy, P., Katta, V. R. and Roquemore, W. M., "A Vortex-Flame Interaction Study Using Four-Wave Mixing Techniques," J. Nonlinear Opt. Phys. Mater., 5(3), (1996), 505.

Hirschfelder, J. O., Curtiss, C. F. and Bird, R. B., Molecular Theory of Gases and Liquids, (1954), Chapters 8 and 9, John Wiley & Sons, Inc., New York.

Hottel, H. C. and Hawthorne, W. R., "Diffusion in Laminar Flame Jets," Third Symposium (International) on Combustion, Flame and Explosive Phenomena, The Combustion Institute, Pittsburgh, PA, (1949), 254-266 .

Hsu, K. Y., Chen, L.-D., Katta, V. R., Goss, L. P. and Roquemore, W. M., "Experimental and Numerical Investigations of the Vortex-Flame Interactions in a Driven Jet Diffusion Flame," AIAA Paper 93-0455, Reno, Jan., 11-16 (1993).

Kaplan, C. R., Oran, E. S., Kailasanath, K. and Ross, H. D., "Gravitational Effects on Sooting Diffusion Flames," 26th Symposium (International) on Combustion, The combustion Institute, Pittsburgh, PA, (1996), 1301-1309 .

Katta, V. R. and Roquemore, W. M., "Role of Inner and Outer Structures in a Transitional Diffusion Flame," Combustion and Flame, 92, 2, (1993), 274-282.

Katta, V. R., Goss, L. P. and Roquemore W. M., "Effect of Nonunity Lewis number and Finite-Rate Chemistry on the Dynamics of a Hydrogen-Air Jet Diffusion Flame," Combustion and Flame, 96, 1-2, (1994a), 60-74.

Katta, V. R., Goss, L. P. and Roquemore, W. M., "Numerical Investigations of Transitional H_2/N_2 Jet Diffusion Flames," AIAA Journal, 32, 1, (1994b), 84-94.

Katta, V. R., Goss, L. P. and Roquemore, W. M., "Simulation of Vortical Structures in a Jet Diffusion Flame," International Journal of Numerical Methods for Heat and Fluid Flow, 4, 5, (1994c), 413.

Katta, V. R. and Roquemore, W. M., "On the Structure of Stretched/Compressed Laminar Flamelet — Influence of Preferential Diffusion," Combustion and Flame, 100, 1, (1995), 61.

Katta, V. R. and Roquemore, W. M., "Numerical Studies on Trapped-Vortex Concepts for Stable Combustion," Trans. ASME: J. Eng. Gas Turb. Power 120, (April, 1998a), 60.

Katta, V. R., Hsu, K. Y. and Roquemore, W. M., "Local Extinction in an Unsteady Methane-Air Jet Diffusion Flame," 27th Symposium (International) on Combustion, The Combustion Institute, Boulder, CO, Aug (1998b). 2-7.

Law, C. K., "Heat and Mass Transfer in Combustion: Fundamental Concepts and Analytical Techniques," Progress in Energy and Combustion Sciences, 10, 3, (1984), 295-318.

Lee, S., Flow-Flame Interactions of Transitional Nitrogen Diluted Hydrogen Jet Diffusion Flames, Ph. D. Thesis, University of Iowa, Iowa City, IA, December (1992).

Leonard, B. P., "A Stable and Accurate Convective Modeling Procedure Based on Quadratic Upstream Interpolation," Computer Methods in

Applied Mechanics and Engineering , 19, 1, (1979), 59-98.

Patnaik, G. and Kailasanath, K., "Numerical Simulations of Burner-Stabilized Hydrogen-Air Flames in Microgravity," Combustion and Flame, 99, 10, (1994), 247-253.

Peters, N. and Williams, F. A., AIAA J. 21:423 (1983).

Peters, N., "Flame Calculations with Reduced Mechanisms —An Outline," in Reduced Kinetic Mechanisms for Applications in Combustion Systems, Lecture Notes in Physics, Vol. 15, (1993), 3-14, Springer-Verlag, New York.

Roquemore, W. M., Chen, L-D., Goss, L. P. and Lynn, W. F., "Structure of Jet Diffusion Flames," Turbulent Reactive Flows, edite d by R. Borghi and S. N. B. Murthy, Lecture Notes in Engineering, Vol. 40, (1989), 49-63, Springer-Verlag, Berlin.

Spalding, D. B., "A Novel Finite Difference Formulation for Difference Expressions Involving Both First and Second Derivatives, " International Journal of Numerical Methods in Engineering , 4, (1972), 551.

Takagi, T. and Xu, Z., "Numerical Analysis of Laminar Diffusion Flames —Effects of Preferential Diffusion of Heat and Species," Combustion and Flame, 96, 1 and 2, (1994), 50-59.

Takagi, T., Yoshikawa, Y., Yoshida, K., Komiyama, M. and Kinoshita, S., "Studies on Strained Nonpremixed Flames Affected by Fla me Curvature and Preferential Diffusion," 26th Symposium (International) on Combustion, The combustion Institute, Pittsburgh, PA, (1996), 1103-1110.

Takahashi, F. and Schmoll, W. J., "Lifting Criteria of Jet Diffusion Flames," Twenty-Third Symposium (International) on Combust ion, The Combustion Institute, Pennsylvania, PA, (1991), 677.

Takahashi, F. and Katta, V. R., "A Numerical Investigation of the Stabilizing Mechanism of Methane Jet Diffusion Flames," AIAA Paper 97-0251, 35th Aerospace Sciences Meeting and Exhibit, January 6-10, Reno, NV, (1997).

Takahashi, F., Schmoll, W. J. and Katta, V. R., "Attachment Mechanisms of Diffusion Flames," 27th Symposium (International) on Combustion, The Combustion Institute, Boulder, CO, Aug. 2-7 (1998).

Vilimpoc, V. and Goss, L. P., "SiC-Based Thin-Filament Pyrometry: Theory and Thermal Properties," Twenty-Second Symposium (Inte rnational) on Combustion, The Combustion Institute, Pittsburgh, PA, (1988), 1907-1914.

Williams, F. A., Combustion Theory - The Fundamentals of Chemically Reacting Flow Systems, (1985), Appendix E, Addison-Wesley Publishing Co., Reading, MA.

Yamashita, H., Kushida, G. and Takeno, T., "A Numerical Study of the Transition of Jet Diffusion Flames," Proceedings of the Ro yal Society of London A, 431, 1882, (1990), 301-314.

Yule, A. J., Chigier, N. A., Ralph, S., Boulderstone, R. and Ventura, J., "Combustion-Transition Interaction in a Jet Flame," A IAA Journal, 19, 6, (1981), 752-760.

Author Profile

William Melvyn "Mel" Roquemore: He received BS degree in Physics in 1963 from Auburn University. After graduation, employed at the Air Force Aero Propulsion Laboratory. Received MS degree in Physics in 1969 from the University of Dayton and Ph.D. degree in Physics from the University of Cincinnati as part of an Air Force Long Term Training Program. Is currently Senior Scientist at the Propulsion Directorate of the Air Force Research Laboratory. Directs experimental and computational research involving fundamental combustion processes and advanced combustor concepts. Is an Air Force Research Laboratory Fellow and has authored 150 publications in combustion and combustion diagnostics.

Viswanath Reddy Katta: He received B.Tech. degree in Electrical Engineering in 1979 from Jawaharlal Nehru Technological University and M.Tech. and Ph.D. degrees in Aerospace Engineering from Indian Institute of Technology, Madras, in 1981 and 1986, respectively. Worked at Nagoya University, Japan, before moving to U.S. in 1989. NRC Post Doctoral Fellow and then employed by SRL before taking current position. Cofounder and Vice-President of Innovative Scientific Solutions Inc. Current interests include simulation of reacting flows, droplet combustion, detonations, vortex dynamics, and fuel thermal stability. Authored more than 150 technical papers in these areas. Associate Fellow of AIAA and member of APS, ASME, and Combustion Institute.